phys. stat. sol. (a) **201**, No. 1, 46–58 (2004) / **DOI** 10.1002/pssa.200306716

Plastic deformation of yttria stabilized cubic zirconia single crystals II. Plastic instabilities

M. Bartsch, A. Tikhonovsky, and **U. Messerschmidt***

Max-Planck-Institut für Mikrostrukturphysik, Weinberg 2, 06120 Halle/Saale, Germany

Received 19 June 2003, revised 6 October 2003, accepted 17 October 2003
Published online 4 December 2003

PACS 61.72.Lk, 62.20.Fe, 81.05.Je, 81.40.Cd, 81.40.Lm, 81.70.Bt

Cubic zirconia with 15 and 20 mol% yttria shows serrated yielding between about 820 °C and 1250 °C. In the instability range, the strain rate sensitivity of the flow stress is zero. There are similarities of the stress dependence of the strain rate between the stress drops during serrations and stress relaxation tests. The stress relaxation curves exhibit a sharp transition from a minimum relaxation rate to zero rate corresponding to complete blocking of the dislocations. The minimum rates follow an Arrhenius-type relationship which divides the ranges of stable and unstable deformation at the low-temperature border of the instability range. The serrated yielding is interpreted as a strain rate softening instability caused by dynamic strain ageing. This results in a flow stress contribution which increases with increasing temperature, thus leading to a high flows stress in a wide temperature range.

1 Introduction

As shown in Part I of this paper [1], cubic zirconia single crystals with more than 10 mol% yttria stabilizer show plastic instabilities as sudden stress drops called serrated yielding during deformation in the soft ⟨112⟩ orientation at certain temperatures and strain rates. Such instabilities have been observed before in cubic zirconia [2]. Plastic instabilities were systematically classified in [3]. According to this, they can occur by strain softening, by a negative strain rate sensitivity (strain rate softening instabilities) or by localized heating (thermomechanical instabilities). The strain rate softening instabilities are frequently connected with the Portevin-LeChâtelier (PLC) effect [4, 5] due to dynamic strain ageing. It was concluded in [2] that the instabilities in zirconia occur if the flow stress exceeds 300 MPa and that they are of thermomechanical nature assisted by structural softening. In the present paper, the unstable plastic behaviour of cubic zirconia is studied in more detail in a wider temperature range by ascertaining the stability borders and by comparing the dynamic deformation properties during the instabilities with those during stress relaxation tests. The experimental details and general deformation properties of the materials are described in Part I of this paper [1].

2 Results of macroscopic testing

2.1 Borders of the instability range

It has been shown previously [6, 7] and in Part I [1] that ZrO_2-10 mol% Y_2O_3 deforms in a stable way along ⟨112⟩ at a strain rate of 10^{-5} s^{-1} in the whole temperature range. The same holds for deformation

* Corresponding author: e-mail: um@mpi-halle.de, Phone: +49 345 5582 927, Fax: +49 345 5511223

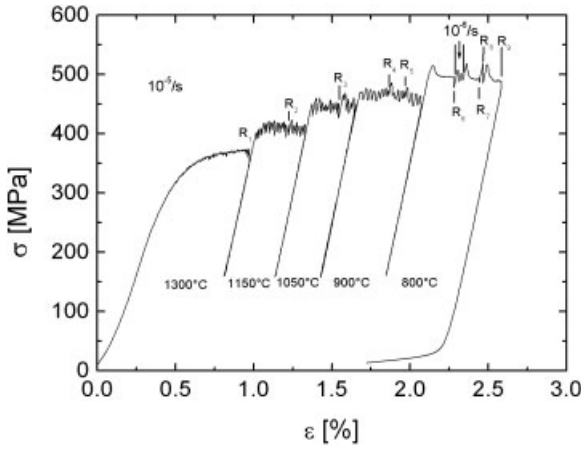

Fig. 1 Stress-strain curve of ZrO_2-15 mol% Y_2O_3 deformed along ⟨112⟩ at a strain rate of 10^{-5} s^{-1} at different temperatures. The section at 800 °C is taken at 10^{-6} s^{-1}. R_n mark stress relaxation tests. All other deformation data in this paper are taken at a ⟨112⟩ compression axis.

along ⟨100⟩ under the same conditions [1]. In ZrO_2 with higher Y_2O_3 contents, in the present study 15 and 20 mol%, plastic instabilities occur at deformation along ⟨112⟩ within a defined temperature range, as demonstrated in Fig. 7 of Part I. This is shown comprehensively also in Fig. 1, which presents the stress σ versus strain ε curve of a ZrO_2-15 mol% Y_2O_3 specimen deformed at a strain rate $\dot{\varepsilon} = 10^{-5}$ s^{-1} at different decreasing temperatures T. The deformation is more or less stable at both 1300 °C and 800 °C but serrated flow occurs between 1150 °C and 900 °C. The temperatures of the stability limits depend on the strain rate. In Fig. 2a, stable deformation at 800 °C changes into unstable one at a decrease of the strain rate from 10^{-5} to 10^{-6} s^{-1}, i.e. with decreasing strain rate, the lower stability border shifts to lower temperatures. The same holds for the upper stability border. This is demonstrated in Fig. 2b, where conversely unstable deformation turns to stable one at the same change of the strain rate. All the data are collected in Fig. 3. It shows the amplitudes of the serrations as a function of both the temperature and the strain rate. The stability borders are indicated by thick lines on the $T-\dot{\varepsilon}$ plane. There seems to be a tendency that the amplitude of the serrations decreases with increasing temperature. In ZrO_2-20 mol% Y_2O_3 specimens, the deformation is still unstable at 1400 °C and becomes stable at 1475 °C. Thus, the upper stability limit is shifted to a higher temperature. The lower stability limit was not observed since the specimens broke below 800 °C. The stability limits seem to depend slightly on the strain. Instability started always at the beginning of plastic deformation. Thus, an incubation strain did not occur. However, near the stability borders, sometimes the deformation turned from unstable to stable after some percent of plastic strain.

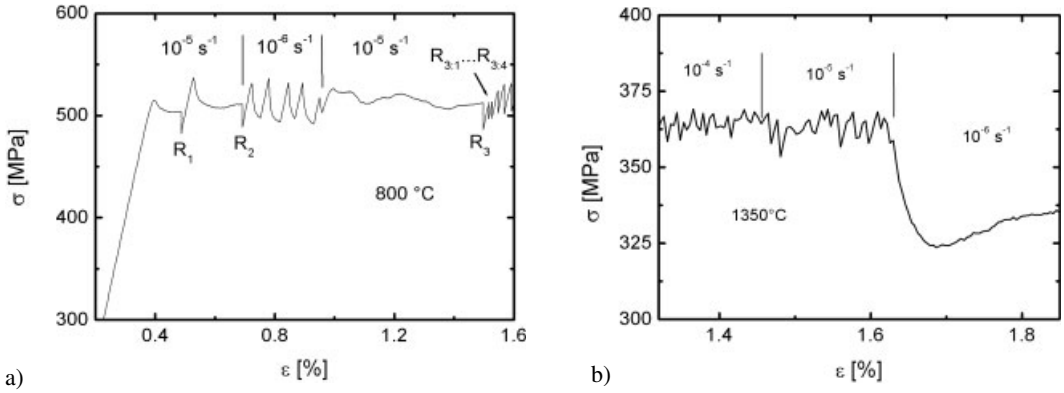

Fig. 2 Sections of stress-strain curves of ZrO_2-15 mol% Y_2O_3 containing changes of the strain rate from 10^{-5} to 10^{-6} s^{-1} which are accompanied with changes of the stability state. a) 800 °C. b) 1350 °C.

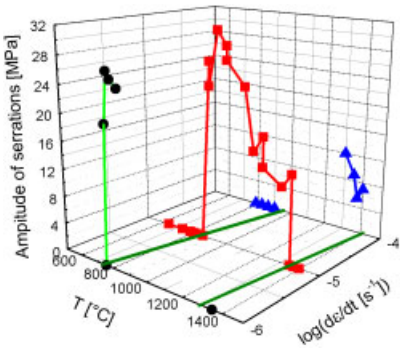

Fig. 3 (online colour at: www.interscience.wiley.com) Dependence of the amplitude of flow stress serrations in ZrO_2-15 mol% Y_2O_3 on temperature and strain rate. The thick lines on the T – log $\dot{\varepsilon}$ plane mark the lower and upper instability borders.

2.2 Shape of the deformation curves in the instability range

Figure 4 presents some sections of deformation curves in the instability range plotted as stress σ versus time t. Figure 4a taken at 860 °C is characteristic also for higher temperatures. First, the stress increases linearly where the slope equals that of the elastic line as measured, e.g., during unloading. The elastic slope is indicated by the straight line. Thus, the loading takes place as purely elastic deformation. After a certain level of stress is reached, plastic deformation sets in at a high rate and the load decreases abruptly. At lower temperatures, plastic deformation does not start at a very high rate so that the unloading parts of the load-time curve gets curved similar to those of stress relaxations, as shown in Fig. 4b for 800 °C. At an even lower temperature in Fig. 4c, also the loading parts become rounded at their tips, which indicates plastic deformation during loading, too.

2.3 Relation between load serrations and stress relaxation tests

As mentioned already in Section 3.1. of Part I [1], stress relaxation curves in the instability range may exhibit instantaneous stress drops which prevent a reliable determination of the strain rate sensitivity. Nevertheless, there exist similarities between the load drops of serrations and stress relaxation tests taken in stable ranges near the instabilities. In both cases, deformation takes place at decreasing load with the only difference that during relaxation tests the deformation is only driven by the relaxing elastic deformation of the load train inside the strain measuring LDTVs which control the driving rate of the testing machine, while at serrated flow the driving rate $\dot{\varepsilon}_m$ of the machine is superimposed. In the latter case, the plastic relaxation rate $\dot{\sigma}_{serr}$ corresponding to the situation during stress relaxation can be calculated by

$$\dot{\sigma}_{serr} = S\dot{\varepsilon}_m - \dot{\sigma}\,, \tag{1}$$

where S is the elastic stiffness of the specimen plus grips over which the driving rate $\dot{\varepsilon}_m$ of the testing machine is controlled and $\dot{\sigma}$ is the stress rate. For stress relaxation, $\dot{\varepsilon}_m = 0$. Figure 5 presents the four serrations of Fig. 2a taken at 800 °C and $\dot{\varepsilon}_m = 10^{-6}$ s^{-1} in the respective plot of ln ($S\dot{\varepsilon}_m - \dot{\sigma}$) versus σ as

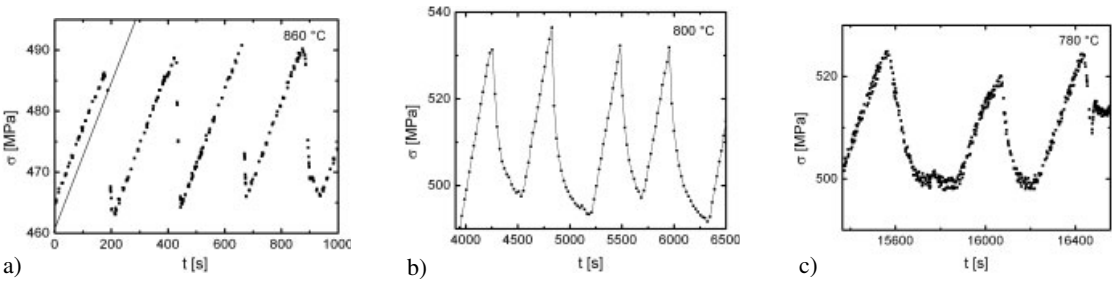

Fig. 4 Stress-time records of the deformation of ZrO_2-15 mol% Y_2O_3 in the instability range at 10^{-6} s^{-1}. a) 860 °C. b) 800 °C. c) 780 °C.

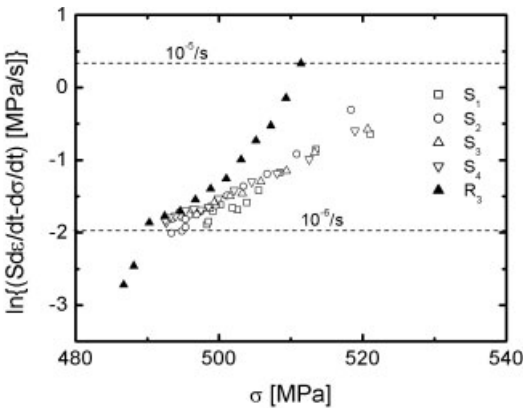

Fig. 5 Comparison between the four serrations of Fig. 2a measured at 800 °C and 10^{-6} s^{-1} and the stress relaxation curve R_3 taken in the following stable part of the deformation curve at 10^{-5} s^{-1}.

well as the relaxation R_3 of the following stable part of the deformation at 10^{-5} s^{-1}. The dotted lines mark strain rates which correspond to the respective stress rates. While at high strain rates, the curves of serrations do not agree with that of the relaxation, both converge at a strain rate of about 10^{-6} s^{-1}. It may be noted that all strain rates during serrations are greater than the drive rate $\dot{\varepsilon}_m$. The relaxation curve has a characteristic shape. At high relaxation rates, the curve has the "inverse" curvature described in Part I, but below a certain rate, the stress remains constant so that the relaxation rate falls steeply down. The different types of relaxation curves at different temperatures are shown in Fig. 6 as stress versus time plots. In the instability ranges, relaxation tests are usually started at a stress just below the tips of the serrations. At 1000 °C with very strong serrations in Fig. 6a, relaxation frequently starts only after an incubation period characterized by the horizontal parts of the curves at the beginning. Afterwards, sudden load drops to lower stress levels occur, sometimes repeatedly. At a higher time resolution, these load drops correspond to sections of relaxation curves. This is more clearly shown in Fig. 6b taken around 800 °C, where the relaxation curves exhibit the behaviour already described with respect to Fig. 5, i.e., the relaxations start in the usual way. After the relaxation rates (slopes of the curves) reach certain minimum values marked by straight lines, the stress remains constant, i.e. the relaxation rates turn to zero. In other words, below the minimum relaxation rates the dislocations become totally blocked so that plastic deformation is not possible at lower rates. In the case of serrations, dislocation motion becomes blocked, too, if the strain rate reaches the minimum rate, and elastic loading starts. Figure 6c presents the normal shape of the relaxation curves in the stable range of deformation at 700 °C, where the stress relaxes to levels lower than that given by the amplitude of serrations.

2.4 Strain rate sensitivity

Stress relaxation curves containing sections of constant stress are not suited to determine the strain rate sensitivity $r = \mathrm{d}\sigma/\mathrm{d}\ln\dot{\varepsilon}$ of the flow stress. Therefore, no strain rate sensitivities were calculated from

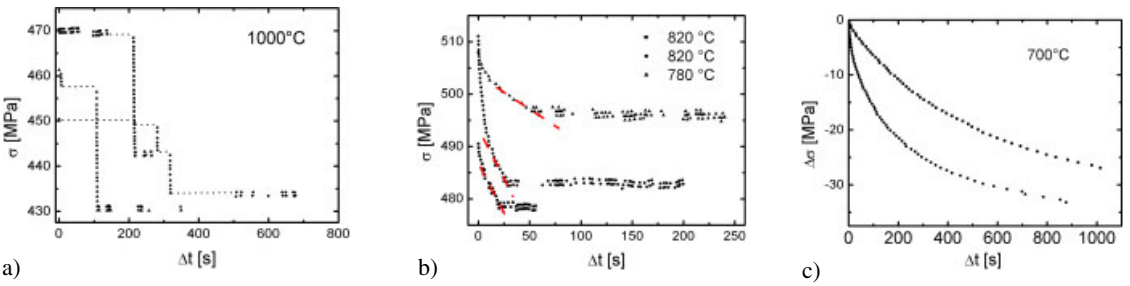

a) b) c)

Fig. 6 (online colour at: www.interscience.wiley.com) Stress versus time curves of relaxation tests of ZrO_2-15 mol% Y_2O_3 at 10^{-5} s^{-1}. a) 1000 °C. b) 820 °C and 780 °C. c) 700 °C.

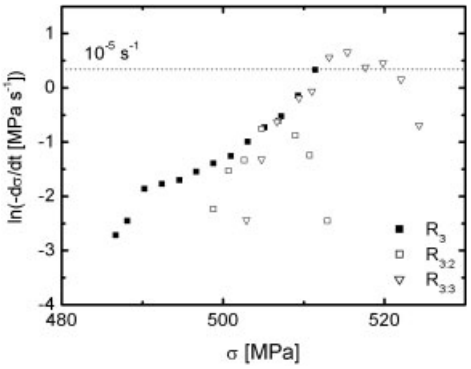

Fig. 7 Stress relaxation curve R_3 of ZrO_2-15 mol% Y_2O_3 taken at 800 °C and $\dot{\varepsilon} = 10^{-5}$ s^{-1} and repeated relaxations $R_{3:2}$ and $R_{3:3}$. The corresponding stress-strain curve is shown in Fig. 2a.

stress relaxations in Part I for the unstable deformation ranges. In the low-temperature stable range, the strain rate sensitivities of both, ZrO_2-15 mol% Y_2O_3 and ZrO_2-20 mol% Y_2O_3, at the beginning of relaxation tests (i.e. in stage 1 of the relaxation curves after the definition in Part I) are equal to those of ZrO_2-10 mol% Y_2O_3 in the same orientation, as shown in Fig. 5 of Part I. At 1400 °C, where the deformation is stable again, the r values in stage 1 of the high yttria materials are substantially lower than those of the ZrO_2-10 mol% Y_2O_3 specimens, but those in stage 2 are equal to them (open symbols in Fig. 5 of Part I).

During the stress relaxation tests, transient effects appear which are expressed by the difference between original relaxation curves starting from steady state conditions and repeated relaxations following the original ones but starting before steady state conditions are reached again. In Fig. 7, the relaxation curve R_3 of Figs. 2a and 5, taken under stable conditions close to the instability range, is re-plotted together with two repeated relaxations, $R_{3:2}$ at a starting stress slightly higher than the original one and $R_{3:3}$ at a higher stress. The repeated relaxation curves start at a low strain rate. Afterwards, the strain rate increases at decreasing stress, reaches a maximum, and then decreases in its usual way. For the second repeated relaxation, the strain rate at the maximum even exceeds the steady state strain rate. The transient effects occurring during the relaxation tests cause a very strong yield point effect if the specimen is deformed again into steady state deformation as demonstrated after relaxation R_1 in Fig. 2a.

In order to obtain data on the strain rate sensitivity also in and near the instability range, some strain rate cycling tests were performed on ZrO_2-15 mol% Y_2O_3 and ZrO_2-20 mol% Y_2O_3 specimens. In the low-temperature stable range of deformation, the stress strain curves at these tests have the shape shown in Fig. 8a. The curve is not very smooth because of the proximity to the instability range. After changing the strain rate, the absolute value of the stress increment first goes through a maximum $\Delta\sigma_{ins}$ and afterwards slowly reaches a steady state value $\Delta\sigma_{ss}$. These increments correspond to the instantaneous strain

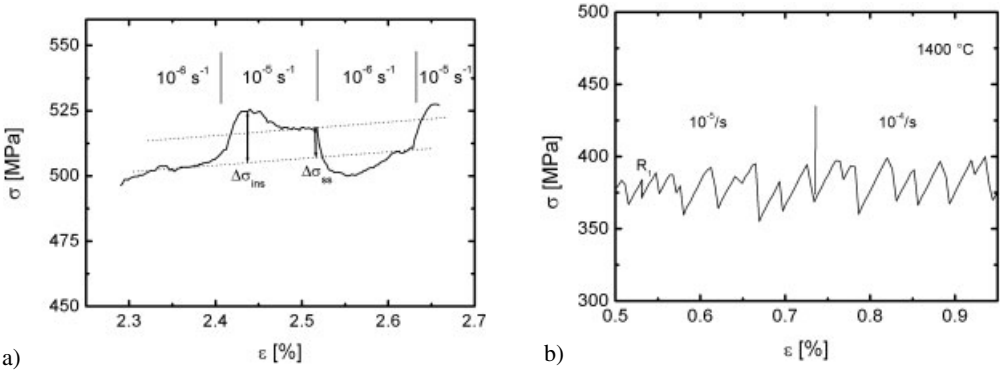

Fig. 8 Sections of stress-strain curves during strain rate cycling experiments. a) Stable deformation of ZrO_2-15 mol% Y_2O_3 at 800 °C, $\dot{\varepsilon} = 10^{-6}$ s^{-1} and 10^{-5} s^{-1}. b) Unstable deformation of ZrO_2-20 mol% Y_2O_3 at 1400 °C with a change of $\dot{\varepsilon}$ from 10^{-5} to 10^{-4} s^{-1}.

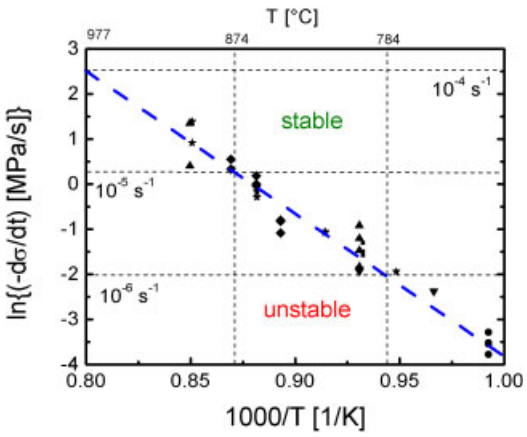

Fig. 9 Arrhenius plot of minimum relaxation rates measured during stress relaxation tests.

rate sensitivity $r_{ins} = \Delta\sigma_{ins}/\Delta \ln \dot{\varepsilon}$ and the steady state one $r_{ss} = \Delta\sigma_{ss}/\Delta \ln \dot{\varepsilon}$. The transition between both is an expression of the transient effects appearing also during stress relaxations. The strain $\Delta\varepsilon_{ss}$ to reach the steady state amounts to about 0.07%, independent of the strain rate. The instantaneous strain rate sensitivity r_{ins} should correspond to that measured by the relaxation tests plotted in Fig. 5 of Part I, which is fulfilled. The steady state values are smaller than the instantaneous ones, $r_{ss} \cong 2/3 r_{ins}$. They are never negative. In the instability range, the transient effects are hidden by the serrated yielding and r is approximately equal to zero as demonstrated by the section of a deformation curve in Fig. 8b with a strain rate change from 10^{-5} to 10^{-4} s^{-1}. There is practically no change in the stress level.

2.5 Activation energy

The minimum relaxation rates described in Section 2.3 depend on the temperature. They are plotted as an Arrhenius diagram in Fig. 9. The experimental data are consistent with a straight line yielding an experimental activation energy of Q = 2.7 eV. As the minimum deformation rates are the limiting rates below which the deformation is blocked, the Arrhenius line in Fig. 9 should describe the lower border of the instability range. The horizontal dashed lines mark again three strain rates corresponding to the respective relaxation rates. Picking a certain temperature on the Arrhenius line, strain rates above the Arrhenius line allow stable deformation while such below the line are impossible since deformation is blocked. Thus, the Arrhenius curve should be identical with the lower border of the instability range in Fig. 3, which is actually true.

3 Discussion

3.1 Theory

Plastic instabilities are discussed theoretically in different degrees of sophistication. Early linear stability analyses of a constitutive model of plastic flow [3, 8–10] have been extended by including transient effects, as reviewed in [11]. A change in the flow stress can then be written as

$$\mathrm{d}\sigma = \Theta\, \mathrm{d}\varepsilon + r\, \mathrm{d} \ln \dot{\varepsilon} + \mathrm{d}\sigma_{\phi}, \tag{2}$$

where Θ is the work hardening coefficient and $\mathrm{d}\sigma_{\phi}$ is a change in the flow stress due to relaxation of an internal parameter ϕ which, after a change in the deformation conditions, reaches a new quasi-steady state value after a characteristic time t_{ϕ}. The inclusion of $\mathrm{d}\sigma_{\phi}$ takes into account the transient effects observed experimentally after changing the deformation conditions, as described in Section 2.4. With a linear approximation of the relaxation process, a linear stability analysis yields the condition for unstable

deformation [11]

$$\frac{1}{t_\phi}\,\frac{r_{\mathrm{ins}}-r_{\mathrm{ss}}}{r_{\mathrm{ins}}} > \frac{\dot{\varepsilon}(\Theta-\sigma)}{r_{\mathrm{ins}}}+\frac{1}{t_\phi}\,. \tag{3}$$

This more general stability criterion includes the criteria of the simpler theories as approximations under simplifying conditions. If it is assumed that the relaxation time t_ϕ is small so that

$$\frac{\dot{\varepsilon}(\Theta-\sigma)}{r_{\mathrm{ins}}} \ll \frac{1}{t_\phi}\,,$$

instability occurs if $r_{\mathrm{ss}} < 0$ at $\Theta - \sigma > 0$. This is equivalent with the adiabatic solution of the constitutive Eq. (2), i.e. with cancelling the term $\mathrm{d}\sigma_\phi$ and setting $r_{\mathrm{ss}} = r$. These kinds of instabilities are called strain rate softening instabilities which may occur if r_{ss} is negative, not r_{ins}, which is always positive. The inequality (3) can also be written as $-r_{\mathrm{ss}} > t_\phi\dot{\varepsilon}\ (\Theta - \sigma)$, where $t_\phi\dot{\varepsilon} = \Delta\varepsilon_{\mathrm{ss}}$. It cannot only be fulfilled by sufficiently negative values of r_{ss}, but also by sufficiently negative values of $\Theta - \sigma$. These kinds of instabilities are called strain softening instabilities.

The different physical processes causing strain rate softening instabilities can be discussed by assigning different physical variables to the structural parameter ϕ. One possibility is to identify ϕ with the local specimen temperature T, since an increase in T yields an increase in the strain rate because of the thermally activated character of the plastic deformation. Thus, instabilities can occur by a feedback between the heat released locally by the plastic deformation and the resulting increase in the strain rate. These instabilities are called thermomechanical instabilities and are a particular case of the strain rate softening instabilities.

In the previous paper on plastic instabilities in zirconia [2], it was concluded that the instabilities are not strain rate softening instabilities, mainly on the basis of the experimental observation that the strain rate sensitivity is not negative, which is also found in the present study. Instead, the instabilities were considered a result of an interplay between thermomechanical and strain softening instabilities, although the criteria for thermomechanical instabilities were failed by orders of magnitude. It is argued in the present paper that the observed instabilities are of the strain rate softening type although r_{ss} is not negative. Therefore, the theory of strain rate softening instabilities is described in more detail.

In alloys, serrated yielding owing to strain rate softening is frequently connected with diffusion processes of alloying elements in the stress fields of the dislocations. This is called dynamic strain ageing as it reduces the dislocation mobility and gives rise to the Portevin-LeChâtelier effect [4, 5]. It is very likely that such effects appear in yttria stabilized zirconia since yttrium ions or vacancies introduced for charge compensation are present in high concentrations and since the occurrence of the plastic instabilities depends on the yttria concentration. Besides, since dynamic strain ageing results in a contribution to the flow stress, it may explain the yttria concentration dependence of the flow stress in a temperature range where recovery is not active any more. The formation of a dynamic cloud of point defects around a moving dislocation was first treated by Cottrell [12]. The theory is outlined here in the version described in Ref. [13]. Owing to a size misfit of solute atoms, an edge dislocation may reduce its energy by acquiring solute concentrations different from the average one in the regions of hydrostatic compression and dilatation. When moving, the dislocation may drag this solute cloud incompletely behind, which causes a velocity depending drag force. At low velocities, the cloud can diffuse easily with the dislocation so that the drag force is small. At high velocities, however, the cloud cannot follow the dislocation anymore and the dragging force is small again. A maximum appears at a critical dislocation velocity

$$v_{\mathrm{c}} = \dot{\varepsilon}_{\mathrm{c}}/(b\rho) = 4DkT_{\mathrm{c}}/\beta\,, \tag{4}$$

where b is the absolute value of the Burgers vector, ρ the dislocation density, D, the diffusion coefficient of the diffusing species, k, the Boltzmann factor and, β, the interaction strength, which is given by

$$\beta = \frac{\mu b(1+\nu)}{3\pi(1-\nu)}\,(V_{\mathrm{s}} - V_{\mathrm{m}})\,. \tag{5}$$

Here, μ is the shear modulus, ν Poisson's ratio, and V_s and V_m are the atomic or ionic volumes of the solute and the matrix atoms or ions. Eq. (4) shows that the critical velocity v_c or the corresponding critical strain rate $\dot{\varepsilon}_c$ increase with increasing temperature, mainly due to the strong temperature dependence of the diffusion coefficient. The maximum contribution of the Cottrell effect to the shear flow stress is approximated to

$$\tau^*_{max} = m_s \sigma_{max} \cong 17 c\beta / b^4 , \tag{6}$$

where m_s is the orientation factor and c is the atomic concentration of the solute.

The models of the Portevin-LeChâtelier effect, as they are reviewed in Ref. [11], use a different approach. It is assumed that the dislocation motion is jerky on a mesoscopic scale owing to obstacles to glide which are overcome by stress assisted thermal activation. During the waiting time at the obstacles, the dislocations are gradually aged by the formation of the solute clouds. This leads to an increase in the activation energy of dislocation motion, which depends on the waiting time t_w [14–16]. According to Ref. [17], the Gibbs free energy of activation can be expressed as

$$\Delta G = \Delta F - V\tau^* + \Delta g \, (1 - \exp \{-(\eta t_w)^n\}) . \tag{7}$$

ΔF is the stress depending free energy of activation, V, the stress dependent activation volume, τ^*, the effective stress, Δg, the increase of the activation energy owing to the ageing, η, the time constant of ageing, and n, an ageing exponent. ΔF and V are supposed to describe the temporary pinning of the dislocations, which is caused by processes different from the diffusing solutes, e.g. by forest dislocations [10]. After the dislocation overcomes the pinned and aged configuration, the activation energy takes the lower value of $\Delta G = \Delta F - V\tau^*$ so that the dislocation may move over a greater distance until it is pinned again. The plastic strain rate is then given by

$$\dot{\varepsilon} = \nu_0 \Omega \exp\left[-\frac{\Delta G}{kT}\right] = \nu_0 \Omega \exp\left[-\frac{\Delta F - V\tau^* + \Delta g(1 - \exp\{-(\eta\Omega/\dot{\varepsilon})^n\})}{kT}\right], \tag{8}$$

ν_0 is a vibrational frequency and Ω an elementary strain, i.e. the strain occurring if all dislocations overcome an obstacle. Here, the waiting time for ageing is set equal to the average waiting time for thermal activation, $t_w = \Omega/\dot{\varepsilon}$. Equation (8) can be solved for $\dot{\varepsilon}$ if the stress dependencies of ΔF and V are known. Figure 10 presents a resulting schematic plot of τ^* versus $\ln \dot{\varepsilon}$. It shows three ranges. In range A at low strain rates, τ^* increases owing to an increasing efficiency of ageing, in range B the dislocations move too fast for effective ageing so that τ^* decreases, finally τ^* increases again in range C due to the increasing resistance of the obstacles which cause the jerky motion. The slope of the curve equals the strain rate sensitivity r, which is positive in range A, negative in range B and positive again in range C. Plastic deformation cannot be stable in range B. Thus, if the macroscopic strain rate corresponds to range B, the specimen may deform at a lower rate in range A, which leads to an increase in τ^*. When τ^* reaches its maximum value at the transition to range B, the deformation can continue at the same stress at a high rate

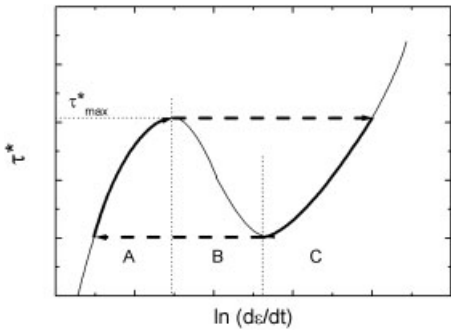

Fig. 10 Schematic plot of the flow stress component resulting from a superposition of thermally activated dislocation glide and dynamic strain ageing as a function of the logarithm of the strain rate.

in range C. This leads to a decrease in τ^* until the transition to range B is reached where the deformation switches back to range A as indicated by the thick broken arrows in Fig. 10. The cycle described corresponds to an increase and stress drop during serrated yielding. Figure 10 also predicts the dependence of the strain rate sensitivity r on the strain rate $\dot{\varepsilon}$ or the stress in the stable ranges. In the normal range C of thermally activated overcoming of obstacles, the curve is bent upwards. This corresponds to an increasing r or a decreasing activation volume $V = lbd$ at increasing stress owing to a decrease of the activation distance d. In the case of Friedel statistics [18, 19], also the obstacle distance l decreases at increasing stress. In the diffusion controlled range A, however, the curve in Fig. 10 must be bent downwards in order to form the maximum at the transition to range B, i.e., r decreases with increasing stress. The dependence of r on the stress is reflected in the shape of stress relaxation curves, as discussed below. Besides, the time dependence of the activation energy as expressed in Eq. (7) leads to transient effects under non-constant deformation conditions.

As described so far, all dislocations may move with the same velocity. The theory reviewed in Ref. [11] includes two important extensions.

– The assumption of equal waiting times t_w for all dislocations is replaced by a distribution function of the waiting times.

– Dislocations moving on parallel slip planes are considered to be coupled by long-range elastic interactions. This leads to a synchronization of the waiting times, i.e., to a collective mode of dislocation motion.

For obtaining plastic instabilities both the occurrence of dynamic strain ageing and the coupling of dislocations are necessary. Thus, the Portevin-LeChâtelier effect consists in a localization of slip in time and space. The most important result of the extended theory is that the strain rate sensitivity r need not be negative as in the earlier theories. It is sufficient if r is close to zero. The low strain rate sensitivity is necessary for the synchronization of the waiting times.

3.2 Comparison with experiments

In Ref. [2], the interpretation of the plastic instabilities in cubic zirconia on the basis of dynamic strain ageing was rejected because negative strain rate sensitivities and static strain ageing near the instability ranges had not been observed, although cubic zirconia contains high concentrations of yttrium ions as solutes and although the occurrence of the instabilities depends on the solute concentration. The present study extends to much lower temperatures. In the material with 10 mol% yttria, which deforms in a stable way at all temperatures, the instantaneous strain rate sensitivity r_{ins}, which is measured at the beginning of stress relaxation curves, drops to very low (positive) values in the respective temperature range, as shown in Fig. 5 of Part I. The materials with higher yttria concentrations, which show the instabilities, have the same low strain rate sensitivity at temperatures below the instability range and still low ones at high temperatures. As described in Section 2.4., the steady state strain rate sensitivity r_{ss} measured in strain rate cycling tests, is lower than the instantaneous one r_{ins} at low temperatures, but not very much, and it is always positive. However, in the instability range, r is zero or very close to zero, as demonstrated by the strain rate changes in Figs. 2b and 8. Thus, the present strain rate sensitivity data do not fulfil the criterion for strain rate softening instabilities according to the earlier theory [8–10] but they do according to the extended one [11]. Plastic instabilities at a strain rate sensitivity close to zero were also observed in other materials [20].

In the following, the occurrence of serrated yielding is discussed on the basis that dynamic strain ageing is due to the diffusion of undissociated yttrium ions. Such an interaction was proposed before [21–23] to explain the plastic behaviour of cubic zirconia above 1400 °C which, according to Part I, should essentially be controlled by recovery. As described already in Part I, the structural vacancies introduced for charge compensation of the aliovalent yttrium ions are too mobile to explain the effects near 1000 °C. In a simplified way, the stability borders can be discussed by the curve in Fig. 10. The curve is valid for a certain temperature. Increasing the temperature shifts the curve to higher strain rates. The minimum between ranges B and C corresponds to the low-temperature stability border. Stable deformation slightly

right of this border in range C becomes unstable by reducing the strain rate into range B or by shifting the curve to the right owing to a higher temperature with the same effect. Similarly, the maximum between ranges A and B corresponds to the high-temperature stability border, where unstable deformation is obtained from the stable range A by either increasing the strain rate or decreasing the temperature. The described transitions are observed in Figs. 1 to 3. Apparently, the condition observed in Ref. [2] that instabilities occur if the flow stress exceeds 300 MPa is not generally valid. In the present study, the flow stress of the materials with 15 and 20 mol% yttria is always higher than 350 MPa independent of the stability status. Besides, the material with 10 mol% yttria reaches very high flow stresses in both orientations at low temperatures without unstable deformation.

Equations (4) to (6) can be used to estimate the properties of the maximum of the curve in Fig. 10. Numerical values are taken from the Appendix of Part I, i.e., the energy factor K_s = 80.4 GPa for the shear modulus μ and the ionic radii of Y^{3+} and Zr^{4+} of 0.102 nm and 0.084 nm, yielding $(V_s - V_m)/b^3$ = 0.0397. Poisson's ratio ν can be set $\nu = 1 - K_s/K_e$ with an energy factor of the edge dislocation K_e = 97.3 GPa [24] so that ν = 0.178. A characteristic dislocation density is $\rho = 10^{13}$ m^{-2} (Fig. 14 of Part I). If it is assumed, as stated above, that the maximum of the curve is identical with the upper instability border at about $T_c \cong 1400$ °C, Eqs. (4) and (5) can be used to estimate the necessary diffusion coefficient for deformation at $\dot{\varepsilon} = 10^{-5}$ s^{-1}. It turns out that $D \cong 6 \times 10^{-19}$ m^2 s^{-1}. This value can be compared with diffusion data, considering that the diffusion coefficient of yttrium should be similar to that of zirconium [25, 26]. The estimated value of D fits well the extrapolated value between the cation diffusion data from the loop shrinkage study in Ref. [27] for ZrO_2-10 mol% Y_2O_3 at lower temperatures and the interdiffusion data [25] at higher ones. Although this is not a proof of the model, it shows that the diffusion of yttrium ions should be fast enough to cause dynamic strain ageing.

Equation (6) gives a rough estimate of the contribution of dynamic strain ageing to the flow stress. With the same data as above, $\tau^*_{max} = 8.25$ GPa $\times c$. According to Ref. [28], the concentration of free yttrium ions in % is given by $c_{Y_{3+}} \cong 2.47\ c_{Y_2O_3}^{0.71}$, where $c_{Y_2O_3}$ is the mole percentage of Y_2O_3. For the concentrations in this study of 10, 15 and 20 mol %, $c_{Y_{3+}}$ amounts to 12.7, 16.9, and 20.7%. With m_s = 0.47 for the ⟨112⟩ specimen orientation and the 15 mol% material, $\sigma_{max} \cong 3$ GPa. This is an order of magnitude higher than the total flow stress. Thus, defects with much weaker interaction are sufficient to cause an essential contribution to the flow stress by dynamic strain ageing. A lower interaction strength β would also lead to a smaller required diffusion coefficient D, which fits the reduced diffusion coefficient of the materials with higher yttria concentrations [27]. The occurrence of dynamic strain ageing may give rise to a flow stress anomaly owing to the maximum in the curve of Fig. 10. In zirconia with high yttrium concentrations, the increasing contribution of dynamic strain ageing to the flow stress at increasing temperature below 1400 °C may compensate the decreasing contributions of other mechanisms so that an almost constant flow stress is obtained like, e.g., in TiAl [29]. At temperatures above the upper border of the instability range, fast cation diffusion results in a decrease of the flow stress by both a decreasing action of dynamic strain ageing and the occurrence of dynamic recovery.

In the present study, the low-temperature border of the instability range in zirconia was detected for the first time. Such limited ranges of instability are typical also for other materials, as reviewed for f.c.c. binary solid solutions in Ref. [30]. This border is connected with the sharp transition between plastic deformation at a minimum rate and complete blocking by full ageing of the dislocations during stress relaxation tests (Fig. 6). At this transition, the velocity of diffusing solutes becomes equal to the velocity of moving dislocations. Thus, the temperature dependence of the minimum rates demonstrated in Fig. 9 is directly connected with the temperature dependence of the underlying diffusion process. There are no cation or solute diffusion data available for temperatures as low as 800 °C. The lowest temperature of 1100 °C was reached by the loop shrinkage data of Ref. [27] with an activation energy of 5.3 eV. The substantially lower activation energy of 2.7 eV observed in Fig. 9 for the dislocation locking may therefore correspond to short-range diffusion in the dislocation cores. This is supported by an activation energy of 3.03 eV for grain boundary yttrium interdiffusion, although measured at much higher temperatures [25]. Thus, the character of the diffusion processes may change from short-range diffusion in the dislocation cores at the low-temperature border to bulk diffusion at the high-temperature one.

The model underlying Eq. (7) requires a jerky dislocation motion controlled by a thermally activated process to pin the dislocations so that strain ageing can occur. In many papers (e.g. [10]), cutting of the dislocation forest is considered such a mechanism. In the course of straining, the elementary strain Ω in Eq. (8) changes, leading to a dependence of the stability state on the strain and the actual flow stress owing to work-hardening, as observed in many studies (e.g. [30, 31]). In the present situation, however, the work-hardening coefficient is very low for the single slip orientation so that the instabilities depend only very weakly on the strain. In particular, there is no critical strain necessary for the instabilities. The low work-hardening coefficient certainly favours unstable deformation according to the inequality (3). However, all the methods for further evaluations based on the stress dependence, e.g., of the strain rate sensitivity cannot be used. It is suggested that in cubic zirconia the overcoming of small precipitates, as discussed in Section 4.6. of Part I, is responsible for the jerky dislocation motion. This process controls the instantaneous strain rate sensitivity, which is independent of the yttria concentration in the low-temperature stable range, where this mechanism is controlling (Fig. 5 of Part I).

An important ingredient of dynamic strain ageing is the occurrence of transient effects at changes of the deformation conditions due to the time dependence of the activation energy in eq. (7). In the low-temperature stable range, these effects are expressed in the difference between original stress relaxation curves started from steady state deformation and repeated relaxation curves started before steady state is reached again. In Fig. 7, the loading between the different relaxation curves is almost elastic. The repeated relaxation curve $R_{3:2}$ starts at approximately the same stress as the original curve R_3 but at a relaxation rate which is more than an order of magnitude lower than the original one. This is due to the almost complete blocking of the dislocations. Slowly, at decreasing stress, the relaxation rate increases. Thus, in this transient range the strain rate sensitivity is negative. Finally, the relaxation rate decreases in its usual way. This kind of repeated relaxation curves was also observed in ZrO_2-10 mol% Y_2O_3 deformed along ⟨100⟩ (Figs. 4a and c of Part I), where the deformation is always stable. Since the serrations start from elastic or almost elastic loading, the strain rate versus stress behaviour corresponds rather to the repeated relaxation curves than to the original ones, cf. Figs. 5 and 7. The ageing of the dislocations leads also to the formation of yield drop effects after a relaxation when the deformation is continued into steady state deformation again. Examples are R_1 in Fig. 2a and R_7 in Fig. 1. Both, these ageing peaks and transient effects at load changes were also observed in ZrO_2-10 mol% Y_2O_3 deformed along ⟨112⟩ [6].

The relation between strain ageing processes and the behaviour of stress relaxation curves was studied before [32, 33]. In the present experiments, an inverse curvature of the stress relaxation curves was observed in stable ranges like the upper part of R_3 in Fig. 5, where the strain rate sensitivity decreases with increasing stress or strain rate. This behaviour can naturally be explained by range A in Fig. 10 with a decreasing slope at increasing strain rate. It is also observed in other materials showing a flow stress anomaly with or without unstable deformation [29, 34] as well as in ZrO_2-10 mol% Y_2O_3 around 1000 °C both along ⟨112⟩ [6] and ⟨100⟩ (Part I, Fig. 4b). This shows that dynamic strain ageing may contribute to the flow stress although the deformation is stable. In addition to dynamic strain ageing, the inverse curvature of relaxation curves may also arise from dynamic recovery. This process was used to explain the deformation behaviour of cubic zirconia at high temperatures [35, 36]. In the present materials with higher yttria concentrations, both processes may superimpose during relaxations around 1400 °C.

Plastic instabilities are always connected with localization of slip in narrow slip bands. This is a necessary condition according to the extended theory reviewed in Ref. [11]. Figure 9 of Part I shows the birefringence patterns of ZrO_2-15 mol% Y_2O_3 specimens deformed at different temperatures. The deformation is localized in few slip bands in the instability range (Part I, Fig. 9a, b) but homogeneous in the stable range at 1400 °C (Part I, Fig. 9c). However, the number of slip bands is clearly lower than the number of serrations so that there is not a one to one correspondence between both. Localized slip is also demonstrated in the transmission electron micrograph of Fig. 15 of Part I. The image shows also several groups of dislocations of the same sign which are in close elastic interaction.

4 Conclusions

– Cubic zirconia with 15 and 20 mol% of yttria exhibits serrated yielding in a limited temperature range between about 800 °C and 1400 °C depending on the strain rate and the yttria concentration.

– The plastic instabilities are accompanied with localized slip and zero strain rate sensitivity as well as stress relaxation curves with inverse curvature and different transient effects in the stable ranges near the unstable ones.

– The instabilities can be explained by dynamic strain ageing owing to the diffusion of unassociated yttrium ions facilitated by low work-hardening, resulting in complete blocking of the dislocations.

– The anomalous increase of the flow stress due to strain ageing compensates its usual decrease yielding a very weak temperature dependence of the flow stress with a value of still about 350 MPa at 1400 °C.

Acknowledgements The authors wish to thank Prof. H. Neuhäuser for critically reading the manuscript. They are also grateful for the cooperation within the framework of the Graduiertenkolleg No. 415 of the Martin-Luther-Universität Halle/Wittenberg and for its financial support by the Deutsche Forschungsgemeinschaft (A.T.).

References

[1] A. Tikhonovsky, M. Bartsch, and U. Messerschmidt, phys. stat. sol. (a) 201, **1** (2004).
[2] K. J. McClellan, A. H. Heuer, and L. P. Kubin, Acta Mater. **44**, 2651 (1996).
[3] Y. Estrin and L. P. Kubin, Res Mech. **23**, 197 (1988).
[4] M. A. LeChâtelier, Rev. Metall. **6**, 914 (1909).
[5] A. Portevin and F. LeChâtelier, Comp. Rend. Sci. Paris **176**, 507 (1923).
[6] B. Baufeld, M. Bartsch, U. Messerschmidt, and D. Baither, Acta Metall. Mater. **43**, 1925 (1995).
[7] B. Baufeld, B. V. Petukhov, M. Bartsch, and U. Messerschmidt, Acta Metall. Mater. **46**, 3077 (1998).
[8] L. P. Kubin and Y. Estrin, J. Phys. (Paris) **47**, 497 (1986).
[9] L. P. Kubin, K. Chihab, and Y. Estrin, Acta Metall. **36**, 2707 (1988).
[10] L. P. Kubin and Y. Estrin, Acta Metall. Mater. **38**, 697 (1990).
[11] M. Zaiser and P. Hähner, phys. stat. sol. (b) **199**, 267 (1997).
[12] A. H. Cottrell, Phil. Mag. **74**, 829 (1953).
[13] J. P. Hirth and J. Lothe, Theory of Dislocations (John Wiley, New York, 1982).
[14] A. van den Beukel, phys. stat. sol. (a) **30**, 197 (1975).
[15] P. G. McCormick, Acta Metall. **36**, 3061 (1988).
[16] T. Wutzke and Ch. Schwinck, phys. stat. sol. (a) **137**, 337 (1993).
[17] N. Louat, Scr. Metall. **15**, 1167 (1981).
[18] J. Friedel, Dislocations (Addison-Wesley, Reading MA, 1964).
[19] U. F. Kocks, A. S. Argon, and M. F. Ashby, Thermodynamics and Kinetics of Slip, Prog. Mater. Sci., Vol. 19 (Pergamon, Oxford et al., 1975).
[20] U. Kettner, H. Rehfeld, C. Engelke, and H. Neuhäuser, Intermetallics **7**, 405 (1999).
[21] D. Gomez-Garcia, J. Martinez-Fernandez, A. Dominguez-Rodriguez, P. Eveno, and J. Castaing, Acta Mater. **44**, 991 (1996).
[22] T. A. Parthasarathy and R. S. Hay, Acta Mater. **12**, 4663 (1996).
[23] D. Gomez-Garcia, J. Martinez-Fernandes, A. Dominguez-Rodriguez, and K. H. Westmacott, J. Am. Ceram. Soc. **80**, 1668 (1997).
[24] U. Messerschmidt, B. Baufeld, and D. Baither, Key Eng. Mater. Vols. **153–154**, 143 (1998).
[25] Y. Oishi, K. Ando, and Y. Sakka, in: Advances in Ceramics, edited by M. F. Yan and A. H. Heuer, Vol. 7 (Am. Ceram. Soc., Westerville OH, 1983), p. 208.
[26] H. Solman, J. Chaumont, C. Dolin, and C. Monty, Ceram. Trans. 24 (Am. Ceram. Soc., Westerville OH, 1991), p. 175.
[27] F. R. Chien and A. H. Heuer, Philos. Mag. A **73**, 2733 (1996).
[28] D. Gomez-Garcia, J. Martinez-Fernandez, A. Dominguez-Rodriguez, and K. H. Westmacott, Phil. Mag. A, **79**, 1839 (1999).
[29] U. Messerschmidt, S. Guder, D. Häussler, and M. Bartsch, Mat. Res. Soc. Symp. Proc. **652**, Y11.6.1 (2001).
[30] Ch. Schwink and A. Nortmann, Mater. Sci. Eng. A **234–236**, 1 (1997).
[31] F. Springer, A. Nortmann, and Ch. Schwinck, phys. stat. sol. (a) **170**, 63 (1998).

[32] H. Flor and H. Neuhäuser, Acta Metall. **28**, 939 (1980).
[33] C. Engelke, J. Plessing, and H. Neuhäuser, Mater. Sci. Eng. A **164**, 235 (1993).
[34] U. Messerschmidt, M. Bartsch, S. Guder, D. Häussler, R. Haushälter, and M. Yamguchi, Intermetallics **6**, 729 (1998).
[35] U. Messerschmidt, B. Baufeld, K. J. McClellan, and A. H. Heuer, Acta Metall. Mater. **43**, 1917 (1995).
[36] B. Baufeld, D. Baither, M. Bartsch, and U. Messerschmidt, phys. stat. sol. (a) **166**, 127 (1998).